Potential dependent structure of an ionic liquid at ionic liquid|water interface probed by x-ray reflectivity measurements

Naoya Nishi[a,*], Tomoya Uruga[b], and Hajime Tanida[b]

[a] *Department of Energy and Hydrocarbon Chemistry, Graduate School of Engineering, Kyoto University, Kyoto 615-8510, Japan*

[b] *Japan Synchrotron Radiation Research Institute, 1-1-1 Kouto, Sayo, Hyogo 679-5198, Japan*

*Correspondence should be addressed

Tel: +81-75-383-2491

Email: nishi.naoya.7e@kyoto-u.ac.jp

[Abstract]

The structure at air interface and water (W) interface of a hydrophobic ionic liquid (IL), trioctylmethylammonium tetrakis[3,5-bis(trifluoromethyl)phenyl]borate ([$TOMA^+$][$TFPB^-$]), has been studied using x-ray reflectometry. Multilayering of ions have been found at the IL|air interface, with the topmost ionic layer having lower density than the IL bulk. For the IL|W interface, x-ray reflectivity data depends on the phase-boundary potential across the IL|W interface. When the phase-boundary potential of W with respect to IL, $\Delta_{\mathrm{IL}}^{\mathrm{W}}\phi$, is +0.20 V, $TFPB^-$ ions are accumulated at the topmost ionic layer on the IL side of the IL|W interface. On the other hand, when $\Delta_{\mathrm{IL}}^{\mathrm{W}}\phi = -0.27$ V, the accumulation of $TOMA^+$ ions occurs with bilayer thickness, which is probably due to local interaction between $TOMA^+$ ions at the topmost layer and at the second layer through interdigitation of their alkyl chains. To quantitatively analyze the x-ray reflectivity data, we construct a model of the electrical double layer (EDL) at the IL|W interface, by combining the Gouy-Chapman-Stern model on the W side and the Oldham model on the IL side. The constructed model predicts that the EDL on the IL side is within the topmost layer for the phase-boundary potentials in the present study, suggesting that the $TOMA^+$ bilayer found at the negative potential results from the local interaction beyond the framework of the present mean-field theory. Even at the positive potential the surface charge density predicted by the EDL theory is significantly smaller than that estimated from x-ray reflectivity data, which implies that densification of the topmost ionic layer leads us to overestimate the surface charge density.

Keywords: ionic multilayer; liquid-liquid interface; ionic liquid-water interface; quaternary ammonium; tetraalkylammonium; tetraphenylborate; modified Verwey-Niessen model

1 Introduction

Liquid-liquid two-phase system composed of water (W) and hydrophobic ionic liquids (ILs), which are liquid salts composed of hydrophobic cations and anions, has potential applications in the fields of electroanalytical chemistry, such as liquid-liquid extraction of ions,[1–9] two-phase electrochemical synthesis,[10–12] ion-selective electrodes,[13–18] and salt bridge.[19,20] Despite the broad applicability of the IL-W two-phase system for electroanalytical chemistry, only a limited number of studies have been reported to obtain the information on molecular-level structure at the IL|W interface. Pioneering studies on the structure at the IL|W interface are molecular dynamics (MD) simulations performed by Lynden-Bell et al.[21] and by Wipff et al.[22–26] Wipff et al. revealed orientation of IL cations, 1-methyl-3-alkylimidazolium ions ($C_n$mim$^+$) at the IL|W interface.[24,26] They suggested that C_4mim$^+$, a cation having short alkyl chain, does not show any preferential orientation at the [C_4mim$^+$]PF_6^-|W interface[24] and [C_4mim$^+$][$C_1C_1N^-$]|W interface[26] ($C_nC_nN^-$ denotes bis(pentafluoroalkanesolfonyl)amide) whereas C_8mim$^+$ with longer alkyl chain tends to be anisotropically orientated with its octyl chain protruding to the IL phase at the [C_8mim$^+$]PF_6^-|W interface.[24] Their works are followed by subsequent MD simulation studies at the IL|W interface by the same group[27–31] and by others,[32–37] focusing on the liquid-liquid extraction,[27,30,31] adsorption of large-size solutes such as polyoxometalates[28,29] and nanoparticles,[35,36] miscibility of IL with W,[32–34] and the interfacial structure.[37] A recent study[37] on the interfacial structure confirmed the orientation of IL cations at the [C_8mim$^+$][$C_1C_1N^-$]|W interface and [C_{12}mim$^+$][$C_1C_1N^-$]|W interface similar to that of C_8mim$^+$ suggested by Wipff et al.[24] Compared to these extensive simulation studies on the IL|W interface, experimental techniques are limited to a few because not many techniques can probe the structure at the IL|W interface, a buried liquid-liquid interface, at a molecular level. Nishi et al. used second harmonic generation (SHG), a second-order nonlinear optical spectroscopy having interface selectivity, to study the IL|W interface.[38,39] They prepared novel ILs based on cations having both high hyperpolarizability (i.e., SHG activity) and high hydrophobicity, to study the orientation of the IL cations at the IL|W interface. Orientation analysis revealed that dodecyl chain of the IL cations is protruding to the IL phase, similar to that proposed by MD.[24,37] Ouchi et al. successfully performed sum frequency generation (SFG) vibrational spectroscopy, which is also one of the interface-selective second-order nonlinear optical spectroscopy, at the [C_4mim$^+$][$C_1C_1N^-$]|W interface and [C_8mim$^+$][$C_1C_1N^-$]|W interface.[40] They revealed that $C_1C_1N^-$ is orientated with the SO_2 moiety pointing toward the W phase at both the interfaces and that more $C_1C_1N^-$ ions tend to be in the C1 (*cis*) conformation when increasing the alkyl chain of the IL cations from C_4mim$^+$ to C_8mim$^+$. They also noted that CH stretching vibrational modes were not observed at the IL|W interface even for [C_8mim$^+$][$C_1C_1N^-$], the IL of the cation with a long alkyl chain, in contrast to the CH modes pronouncedly appeared at the air interface of the ILs. The disappearance of the CH modes at the IL|W interface seems to be due to the counter orientation of the topmost-layer cations and the second-layer cations, causing the cancellation of the SFG signals for the CH modes.

Since ILs are composed of ions and may be regarded as dense electrolyte solutions, electrochemical

point of view is important to consider the structure of the IL|W interface. There exists phase-boundary potential across the IL|W interface and electrical double layers (EDLs) are formed on both IL and W sides of the interface.[41–43] Local ion concentrations in EDLs are generally different from those in bulk. Electrocapillarity (dependence of surface tension on the phase-boundary potential) studies[44–49] at the IL|W interface confirmed fundamental features of the EDL such as surface excess and specific and non-specific adsorption of IL ions at the IL|W interface. These studies suggested that the EDL at the IL|W interface is not far from the view of the Gouy-Chapman-Stern model[50–52] that has long been the theoretical basis for EDL at the electrochemical interfaces such as electrode|electrolyte solution interface.

The EDL in IL is known to have several unique structures such as layering of ions[53–61] and transition of the ionic layer to solid-like phase.[58,62–64] Such unique structures seem to be the cause for ultraslow dynamics of the interfacial structure at the IL|W interface[65–68] and the IL|electrode interface.[69–73] Charging properties are also unique; "lattice saturation" and "overscreening" are theoretically proposed[74] and experimentally confirmed.[54,75] The former results from the excluded volume effect between ions in the EDL, not that between ions and electrode that the Gouy-Chapman-Stern model takes into account.[52] The latter is the formation of alternately charged ionic multilayers due to coulombic interaction between neighboring ions. Because of these interesting phenomena that ILs have presented, it should be worth to investigate the EDL at the IL|W interface by a technique having interfacial selectivity at a molecular level. X-ray reflectometry (XR) is a suitable technique for the purpose. Extensive XR studies by Schlossman et al. have already been performed for the EDL at the electrochemical oil-water interface, where the two liquid phases contain electrolyte ions and the phase-boundary potential can be controlled.[76–81] They revealed that the conventional EDL theory, which includes only coulombic interaction between ions via averaged electric potential, is insufficient to elucidate their XR data and that ion-solvent potential of mean force and ion-ion correlation potential play a crucial role in the ion distribution especially in the EDL in oil. In this paper, we introduce a XR study at air and water interface of a hydrophobic IL, trioctylmethylammonium tetrakis[3,5-bis(trifluoromethyl)phenyl]borate ([$TOMA^+$][$TFPB^-$]). We will show that XR can probe the phase-boundary-potential dependent structure in the EDL on the IL side of the IL|W interface.

2 Experimental and theoretical

2.1 Preparation of ionic liquid

[$TOMA^+$][$TFPB^-$] was prepared from [$TOMA^+$]Cl^- (TCI) and Na^+[$TFPB^-$],[7,82] and purified using the same method for [$TOMA^+$][$C_4C_4N^-$] described elsewhere.[57] Na^+[$TFPB^-$] was synthesized using a procedure similar to that previously reported by Nishida et al.[83] from 3,5-bis(trifluoromethyl)bromobenzene and sodium tetrafluoroborate.

2.2 X-ray reflectivity measurement

XR measurements were performed at the beamline BL37XU of SPring-8 using a liquid interface reflectometer.[84] The details of the XR measurements are described elsewhere.[57,59] Briefly, X-ray of 25 keV from the undulator was irradiated to the air or water interfaces of [TOMA$^+$][TFPB$^-$]. The PTFE coated aluminum trough was set on an aluminum block in which temperature-controlled water was flowed. The lower part of the trough was filled with [TOMA$^+$][TFPB$^-$]. The upper part was filled with an aqueous solution for the measurements for the IL|W interface. Temperature was controlled to be 330 K, which is well above the melting point of [TOMA$^+$][TFPB$^-$] (313 K), with an accuracy of 1 K.

The intrinsic surface structure factor, ϕ, as a function of the surface-normal component of the scattering vector, q, was evaluated from the experimentally obtained x-ray reflectivity, R, using the following equation,[57,85]

$$|\phi|^2 = \frac{R}{R_\mathrm{F}} \exp\left[\sigma_\mathrm{CWT}^2 q^2\right] \tag{1}$$

where R_F is the Fresnel reflectivity and σ_CWT is surface roughness due to thermal capillary waves derived from the capillary wave theory. R_F and σ_CWT were calculated using the procedure described elsewhere.[57,59]

The q dependence of ϕ was fitted with model functions using the following equation assuming the kinematic approximation,[85]

$$\phi = \frac{1}{\Delta\rho} \int_{-\infty}^{\infty} \frac{\mathrm{d}\rho}{\mathrm{d}z} \exp\left[iqz\right] \mathrm{d}z, \tag{2}$$

where z is a displacement along the surface normal with $z = 0$ for the interfaces and $z > 0$ for the IL phase, and ρ is the intrinsic electron density averaged in the xy direction (along the surface plane) as a function of z. The electron density difference between two phases, $\Delta\rho$, is ρ_IL for IL|air interface and $\rho_\mathrm{IL} - \rho_\mathrm{W}$ for IL|W interface. $\rho_\mathrm{IL} = 0.373$ e Å^{-3} and $\rho_\mathrm{W} = 0.334$ e Å^{-3} were estimated with molecular weights, densities, and number of electrons for IL and W. The ρ_IL value is the average of those for TOMA$^+$ and TFPB$^-$ in the IL, $\rho_\mathrm{C} = 0.247$ e Å^{-3} and $\rho_\mathrm{A} = 0.499$ e Å^{-3}; $\rho_\mathrm{IL} = (\rho_\mathrm{C} + \rho_\mathrm{A})/2$. The difference between ρ_C and ρ_A enables us to detect the EDL in IL by XR; local concentration change for the IL cation and anion leads to electron density in the EDL different from that in the IL bulk.

2.3 EDL calculation

We performed a model calculation for the electrical double layer (EDL) at the IL|W interface. The basic idea of the model is the same as the modified version[86] of the Verwey-Niessen model[87] for oil|water interface. The modified Verwey-Niessen model consists of two EDLs of the Gouy-Chapman-Stern type on the oil and water sides of the oil|water interface. The modification means that the modified Verwey-Niessen model[86] incorporates ion-free "inner layer" at the both side of the interface in which ions cannot enter, similarly to the Stern layer at the electrode|electrolyte solution interface. The thickness of the inner layer on the W side is the radius of

solvated ions in W usually set to 0.3 nm. On the oil side, the inner layer is thicker than that for W, because generally hydrophobic electrolyte ions in oil are big and have symmetric shape, and the charged part is located inside the ions. The incorporation of the inner layers succeeded in the explanation of the EDL behavior at the oil|water interface.[88] In the present study for the IL|W interface, we adopted the EDL model proposed by Oldham[89] for the IL side of the interface, instead of the Gouy-Chapman-Stern model used for the EDL on the oil side of the oil-water interface, to incorporate the excluded volume effect between IL ions. We adopted the inner layer thicknesses for IL and W to be $d_{\mathrm{surf}}/2$ (the ion radius) and 0.3 nm, respectively. We neglect specific adsorption of ions at the IL|W interface from the previous experimental evidences.[46,49]

Suppose that the IL|W interface is located at $z = 0$, and the IL and W sides of the interface are $z > 0$ and $z < 0$, respectively. We neglect specific adsorption of ions at the IL|W interface from the previous experimental evidences.[46,49] The ion-free inner layers (the Stern layers) exist on the IL and W sides of the interface with a thickness of $d_{2,\mathrm{IL}}$ and $d_{2,\mathrm{W}}$, respectively. To fulfill the electroneutrality for the EDLs, the surface charge density on the IL and W sides, $q_{\mathrm{IL}} \equiv \int_{d_{2,\mathrm{IL}}}^{\infty} \mathrm{d}z\, \rho_{\mathrm{C}}(z)$ and $q_{\mathrm{W}} \equiv \int_{-\infty}^{-d_{2,\mathrm{W}}} \mathrm{d}z\, \rho_{\mathrm{C}}(z)$, should have equal magnitude but opposite sign

$$q_{\mathrm{W}} = -\, q_{\mathrm{IL}} \tag{3}$$

where $\rho_{\mathrm{C}}(z)$ is the volume charge density at z. For the EDL calculation at the IL|W interface, this liquid-liquid system composed of the two EDLs can be decomposed into two electrode-liquid systems each of which has one EDL on the liquid side of the electrode|liquid interface. The EDL on the W side of IL|W interface is the same as the EDL for electrode|water interface at $q_{\mathrm{M}} = q_{\mathrm{IL}}$ where q_{M} is the surface charge density at the electrode surface. Similarly, the IL EDL for IL|W interface is the same as the EDL of electrode|IL interface at $q_{\mathrm{M}} = -q_{\mathrm{IL}}$.

We shall define x, another coordinate along the surface normal of the electrode|water and electrode|IL interfaces with $x = 0$ for the electrode surface and $x > 0$ for the liquid phase,

$$x = \begin{cases} +z & (z \geq 0,\ \text{EDL in IL}) \\ -z & (z \leq 0,\ \text{EDL in W}) \end{cases} \tag{4}$$

and also define the potential profile at the electrode|water and electrode|IL interfaces as $\phi_{\mathrm{M/W}}(q_{\mathrm{M}}, x)$ and $\phi_{\mathrm{M/IL}}(q_{\mathrm{M}}, x)$, respectively, taking a reference that $\phi_{\mathrm{M/W}}(q_{\mathrm{M}}, \infty) = \phi_{\mathrm{M/IL}}(q_{\mathrm{M}}, \infty) = 0$.

The phase-boundary potential at the IL|W interface as a function of q_{IL}, $\Delta_{\mathrm{IL}}^{\mathrm{W}}\phi(q_{\mathrm{IL}})$, can be written as

$$\Delta_{\mathrm{IL}}^{\mathrm{W}}\phi(q_{\mathrm{IL}}) = \phi_{\mathrm{M/IL}}(-q_{\mathrm{IL}}, 0) - \phi_{\mathrm{M/W}}(q_{\mathrm{IL}}, 0) \tag{5}$$

The potential profile at the IL|W interface, $\phi_{\mathrm{W/IL}}(q_{\mathrm{IL}}, z)$ is

$$\phi_{\mathrm{W/IL}}(q_{\mathrm{IL}}, z) = \begin{cases} \phi_{\mathrm{M/IL}}(q_{\mathrm{IL}}, x) & (z \geq 0,\ \text{EDL in IL}) \\ \Delta_{\mathrm{IL}}^{\mathrm{W}}\phi(q_{\mathrm{IL}}) - \phi_{\mathrm{M/W}}(-q_{\mathrm{IL}}, x) & (z \leq 0,\ \text{EDL in W}) \end{cases} \tag{6}$$

The potential profile can be represented as a inverse function, i.e., $z(\phi_{\mathrm{W/IL}}, q_{\mathrm{IL}})$, with the decomposition to four

parts (two diffusion layers and two inner layers for IL and W) with $\phi_{\mathrm{M/IL}}$ or $\phi_{\mathrm{M/W}}$ as a parameter.[89]

$$z(\phi_{\mathrm{W/IL}}, q) = x_{\mathrm{M/IL,diffuse}}(\phi_{\mathrm{M/IL}}, q) \tag{7}$$

$$= d_{2,\mathrm{M/IL}} - \mathrm{sgn}(q)\kappa^{-1} \int_{\phi_{2,\mathrm{M/IL}}(q)}^{\phi_{\mathrm{M/IL}}} \mathrm{d}\left(\frac{F\phi'}{RT}\right) \frac{1}{\sqrt{2\ln\left[\cosh\left(\nu\frac{F\phi'}{RT}\right)\right]}}$$

$$(z \geq d_{2,\mathrm{M/IL}}, \text{diffuse layer in IL}) \tag{8}$$

$$z(\phi_{\mathrm{W/IL}}, q) = x_{\mathrm{M/IL,inner}}(\phi_{\mathrm{M/IL}}, q) \tag{9}$$

$$= d_{2,\mathrm{M/IL}} \frac{\phi_{\mathrm{M/IL}} - \phi_{0,\mathrm{M/IL}}(q)}{\phi_{2,\mathrm{M/IL}}(q) - \phi_{0,\mathrm{M/IL}}(q)}$$

$$(0 \leq z \leq d_{2,\mathrm{M/IL}}, \text{inner layer in IL}) \tag{10}$$

$$z(\phi_{\mathrm{W/IL}}, q) = -x_{\mathrm{M/W,inner}}(\phi_{\mathrm{M/W}}, -q) \tag{11}$$

$$= -d_{2,\mathrm{M/W}} \frac{\phi_{\mathrm{M/W}} - \phi_{0,\mathrm{M/W}}(-q)}{\phi_{2,\mathrm{M/W}}(-q) - \phi_{0,\mathrm{M/W}}(-q)}$$

$$(-d_{2,\mathrm{M/W}} \leq z \leq 0, \text{inner layer in W}) \tag{12}$$

$$z(\phi_{\mathrm{W/IL}}, q) = -x_{\mathrm{M/W,diffuse}}(\phi_{\mathrm{M/W}}, -q) \tag{13}$$

$$= -d_{2,\mathrm{M/W}} - \kappa^{-1} \ln\left\{\frac{\tanh\left(\frac{\nu}{4}\frac{F\phi_{2,\mathrm{M/W}}(-q)}{RT}\right)}{\tanh\left(\frac{\nu}{4}\frac{F\phi_{\mathrm{M/W}}}{RT}\right)}\right\}$$

$$(z \leq -d_{2,\mathrm{M/W}}, \text{diffuse layer in W}) \tag{14}$$

where $\phi_{0,\mathrm{j}}(q) = \phi_{\mathrm{j}}(q, 0)$, $\phi_{2,\mathrm{j}}(q) = \phi_{\mathrm{j}}(q, d_{2,\mathrm{j}})$ (j=M/IL or M/W), $\kappa^{-1} = \sqrt{\frac{RT\epsilon\epsilon_0}{2F^2c_0}}$ is the Debye length and sgn is the sign function.

The z dependence of the ionic concentrations in IL and W, $c_{\mathrm{i,IL}}(z)$ and $c_{\mathrm{i,W}}(z)$, respectively, is obtained using $\phi_{\mathrm{W/IL}}$ as a parameter, as follows,

$$c_{\mathrm{i,W}}(z) = c_{0,\mathrm{W}} \exp\left\{-\nu_{\mathrm{i}} \frac{F\phi_{\mathrm{W/IL}}(z)}{RT}\right\} \qquad (z \leq -d_{2,\mathrm{M/W}}, \text{diffuse layer in W}) \tag{15}$$

$$c_{\mathrm{i,IL}}(z) = c_{0,\mathrm{IL}} \frac{\exp\left(-\mathrm{sgn}(\nu_{\mathrm{i}})\nu_{\mathrm{i}}\frac{F\phi_{\mathrm{W/IL}}}{RT}\right)}{\cosh\left(\nu_{\mathrm{i}}\frac{F\phi_{\mathrm{W/IL}}}{RT}\right)} \qquad (z \geq d_{2,\mathrm{M/IL}}, \text{diffuse layer in IL}) \tag{16}$$

We calculated the potential and concentration profiles by numerically solving the above equations with Mathematica. The parameters used are listed in Table 1.

3 Results and Discussion

3.1 XR at the IL|air interface

First, we measured XR at the IL|air interface to reveal the surface structure of [TOMA$^+$][TFPB$^-$]. Fig.1a shows the q^2-dependent plots of the intrinsic surface structure factor ($\log|\phi|^2$) for the [TOMA$^+$][TFPB$^-$]|air interface. The $\log|\phi|^2$ values are less than 0 for all the q range studied, which qualitatively means that a low-electron

density region exists at the surface. This tendency is opposite to those previously obtained for the surface of other hydrophobic ILs,[57,59] where a quasi-Bragg peak resulting from ionic multilayers was observed. To quantitatively analyze the XR data, we fitted several models to the data and compared the resultant values of Akaike's information criterion (AIC),[90] a measure of likelihood of models. One model is the modified distorted crystal (MDC) model[91–93] that includes multilayer characteristics at the surface.

$$\rho = \rho_{\mathrm{IL}} \frac{d}{\sqrt{2\pi}} \left(\frac{f_{\mathrm{surf}}}{\sigma_{\mathrm{surf}}} \exp\left[\frac{-(z - z_{\mathrm{surf}})^2}{2\sigma_{\mathrm{surf}}^2} \right] + \sum_{n=1}^{\infty} \frac{1}{\sigma_n} \exp\left[\frac{-(z - nd)^2}{2\sigma_n^2} \right] \right) \tag{17}$$

where d is the interlayer distance and σ_n is the line width for nth layer. The deeper the position of the layer into bulk, the wider the line width; $\sigma_n^2 = n\bar{\sigma}^2 + \sigma_0^2$ where σ_0 is the line width for the topmost (0th) layer and $\bar{\sigma}$ is a factor of the widening of the distribution. In this model, the normalized electron density, the roughness, and the position of the topmost layer (f_{surf}, σ_{surf}, and z_{surf}, respectively) can be different from those in the normal distorted crystal model where $f_{\mathrm{surf}} = 1$, $\sigma_{\mathrm{surf}} = \sigma_0$, and $z_{\mathrm{surf}} = 0$. Note that in the MDC model each ionic layer is composed of the same number of cation and anion. Because the IL|air interface is not charged, no charge imbalance in an ionic layer occurs. This was previously confirmed for the surface of other hydrophobic ILs.[57,59] Also for the present case of the [$TOMA^+$][$TFPB^-$]|air interface, the model for alternate cation and anion layers for charged interface of IL[54] failed to reproduce the XR data. As a model other than the MDC model, the box model (see Supporting Information) was also fitted to the data. Among the several models and several constraint conditions for the fitting, the MDC model with a constraint $z_{\mathrm{surf}} = 0$ was found to be most likely (Supporting Information). The electron density profile for the case is shown as solid line in Fig.1b and the obtained parameters are listed in Table 2. In Fig.1b one can see ionic multilayers with the topmost layer having low electron density, by comparing to the dashed line in Fig.1b which is a hypothetical electron density profile without the lowering effect. The ionic interlayer distance, d, is 12.0 Å, which is in good agreement with 10.7 Å, the average of the diameters for $TOMA^+$ and $TFPB^-$ estimated from ionic volumes using quantum chemical calculation with an assumption of their spherical shape. The f_{surf} value, 0.77, demonstrates that the topmost ionic layer has low electron density. Such density change in the topmost layer was not observed for the ionic multilayers at the surface of [$TOMA^+$][$C_4C_4N^-$],[57] another hydrophobic IL having the common $TOMA^+$ cation to [$TOMA^+$][$TFPB^-$]. The difference between two anions, $TFPB^-$ and $C_4C_4N^-$ is that $TFPB^-$ is a rigid and symmetrical ion whereas $C_4C_4N^-$ is relatively asymmetrical having two flexible perfluorobutyl moieties. It is expected that more flexible and asymmetric $C_4C_4N^-$ can accommodate to the topmost layer where there exist two-dimensional geometric constraint and dielectric constraint near the air phase with a low permittivity. Therefore, the rigidity and structure symmetricity of $TFPB^-$ is possibly the cause of the low electron density of the topmost layer at the [$TOMA^+$][$TFPB^-$]|air interface.

3.2 XR at the IL|W interface

The EDL structure (ion distribution) at the IL|W interface depends on the phase-boundary potential across the interface. Therefore, we should measure x-ray reflectivity with the phase-boundary potential controlled.

The [TOMA$^+$][TFPB$^-$]|W interface is electrochemically polarizable within 0.8 V,[82] which means that we can control the phase-boundary potential via externally applying voltage between two reference electrodes inserted in IL and W phases,[82] respectively, or internally partitioning common ions between the two phases.[94] We adopted the latter method; we controlled the phase-boundary potential by adding Na$^+$[TFPB$^-$] or [TOMA$^+$]Cl$^-$ into W for the ion partition where TFPB$^-$ or TOMA$^+$ is the common ion, respectively. The Nernst equation for the ion partitions between IL and W to represent the phase-boundary potential, $\Delta^{\mathrm{W}}_{\mathrm{IL}}\phi$ ($\equiv \phi^{\mathrm{W}} - \phi^{\mathrm{IL}}$) is[94]

$$\Delta^{\mathrm{W}}_{\mathrm{IL}}\phi = \Delta^{\mathrm{W}}_{\mathrm{IL}}\phi^{0'}_{\mathrm{i}} - \frac{RT}{z_{\mathrm{i}}F}\ln c^{\mathrm{W}}_{\mathrm{i}} \tag{18}$$

where $\Delta^{\mathrm{W}}_{\mathrm{IL}}\phi^{0'}_{\mathrm{i}}$ is the formal potential of the partition of ion i for IL-W two-phase system, $c^{\mathrm{W}}_{\mathrm{i}}$ is the concentration of i in W, z_{i} is the charge number of i, R is the gas constant, T is the absolute temperature, and F is the Faraday constant. Since we are interested in the EDL on the IL side of the interface, not that on the W side, $c^{\mathrm{W}}_{\mathrm{i}}$ should be low enough otherwise accumulation and depletion of ions in the EDL in W could change the electron density of the EDL from W bulk to a level detectable by XR. To satisfy such a condition, we added 0.01 mM Na$^+$[TFPB$^-$] or 0.1 mM [TOMA$^+$]Cl$^-$ in W. We checked the invariance of electron density on the W side of the interface (Supporting Information). We calculated the phase-boundary potential to be +0.20 V and −0.27 V, respectively, by using eq 18 and the formal potentials for nitrobenzene-W two-phase system as a good measure of $\Delta^{\mathrm{W}}_{\mathrm{IL}}\phi^{0'}_{\mathrm{i}}$ (Table 3).[15,95,96]

Fig.2a shows plots for $\log|\phi|^2$ as a function of q^2 when $\Delta^{\mathrm{W}}_{\mathrm{IL}}\phi = +0.20$ (red circle) and -0.27 (blue square) V. As we expected, $\log|\phi|^2$ depends on $\Delta^{\mathrm{W}}_{\mathrm{IL}}\phi$, reflecting the $\Delta^{\mathrm{W}}_{\mathrm{IL}}\phi$ dependence of the EDL structure in IL. The $\log|\phi|^2$ values increase with increasing q^2 for $\Delta^{\mathrm{W}}_{\mathrm{IL}}\phi = +0.20$ V, suggesting that electron density of the IL side of the interface higher than IL bulk (or that of the W side of the interface lower than W, but we can neglect possibility of the change in electron density of the W side in the present condition). At $\Delta^{\mathrm{W}}_{\mathrm{IL}}\phi = +0.20$ V the IL side of the interface is negatively charged and, therefore, the local concentration of TFPB$^-$ and TOMA$^+$ in EDL in IL is higher and lower than the bulk concentration, respectively. Since electron density of TFPB$^-$ (0.499 e Å^{-3}) is higher than that of TOMA$^+$ (0.247 e Å^{-3}), the electron density of EDL is higher than IL bulk, explaining the experimental data qualitatively. The situation for $\Delta^{\mathrm{W}}_{\mathrm{IL}}\phi = -0.27$ V can be explained oppositely. X-ray reflectivity data at −0.27 V (Fig.2a) shows decrease in $\log\phi^2$ which means low-electron density layer resulting from low-electron density TOMA$^+$ accumulation and high-electron density TFPB$^-$ depletion in the EDL of IL. These tendency was also observed in XR studies of electrochemical oil-water interface, where oil contains hydrophobic electrolyte composed of low electron density cation and high electron density anion.[79–81]

We performed model fitting for the x-ray reflectivity data at the IL|W interface. XR data at the IL|W interface are limited to be relatively in a narrow q range compared with those at the IL|air interface (compare q^2 values in Figs. 1a and 2a). This is due to relatively small electron density difference between IL and W phases which form the IL|W interface, leading to steeper decrease in the Fresnel reflectivity with increasing q and to narrower q range within which x-ray reflectivity is higher than the lower detection limit . The limited q range humpers us to discuss ionic multilayers at the IL|W interface. However, we can discuss the electron density

at topmost ionic layer (the ionic layer closest to the IL|W interface) from the XR data at the IL|W interface. Judging from the AIC values of several models, we analyzed data with one-box model that has a small number of fitting parameters;

$$\rho = \rho_{\mathrm{W}} + (\rho_{\mathrm{int}} - \rho_{\mathrm{W}})\left(\frac{1 + \mathrm{erf}\left[\frac{z}{\sqrt{2}\sigma_{\mathrm{int-W}}}\right]}{2}\right) + (\rho_{\mathrm{IL}} - \rho_{\mathrm{int}})\left(\frac{1 + \mathrm{erf}\left[\frac{z-d_{\mathrm{int}}}{\sqrt{2}\sigma_{\mathrm{int-IL}}}\right]}{2}\right) \quad (19)$$

where ρ_{int} and d_{int} are the electron density and thickness of the "box" (layer) that represents the EDL in IL. In order to limit the number of parameters, the interfacial roughness on the both sides of the box, $\sigma_{\mathrm{int-W}}$ and $\sigma_{\mathrm{int-IL}}$ were set to be equal to σ_{surf} from the result for the [TOMA$^+$][TFPB$^-$]|air interface.

The fitted parameters are listed in Table 3 and the resultant electron density profiles are shown as solid and dashed lines in Fig.2b. The values of d_{int}, the EDL thickness, were 11.7 and 25.5 Å for $\Delta_{\mathrm{IL}}^{\mathrm{W}}\phi$ = +0.20 and −0.27 V, respectively. Compared to 12.0 Å, the ionic layer thickness at the IL|air interface, the former value at +0.20 V corresponds to monolayer thickness and the latter at −0.27 V to bilayer thickness. The fittings for the opposite situation, i.e., bilayer thickness for the former (+0.20 V) and monolayer thickness for the latter (−0.27 V), cannot reproduce the experimental data as shown as dotted and dotted-dashed lines in Fig.2a, respectively. The bilayers are formed at $\Delta_{\mathrm{IL}}^{\mathrm{W}}\phi$ = −0.27 V when TOMA$^+$ is accumulated and TFPB$^-$ is depleted on the IL side of the IL|W interface. Layering of TOMA$^+$ has been discussed in a previous small angle x-ray scattering study in TOMA$^+$-based IL and the derivatives, where alkyl chains from neighboring layers are proposed to be interdigitated.[97] Also, a recent MD study at the IL|W interface suggested that IL-cations at the topmost layer and the second layer have opposite orientations with the alkyl chains for the topmost layer toward IL bulk and those for the second layer toward the topmost layer, forming an alkyl rich region in between the two layers.[37] Therefore, we speculate that the topmost layer is firstly accumulated by TOMA$^+$ when the interface starts to be charged up from $\Delta_{\mathrm{IL}}^{\mathrm{W}}\phi$ = 0 V toward −0.27 V and then the accumulated TOMA$^+$ ions at the topmost layer induce subsequent accumulation at the second layer to form bilayer structure. On the other hand, without motive force to form bilayer for TFPB$^-$ ions, when $\Delta_{\mathrm{IL}}^{\mathrm{W}}\phi$ = +0.20 V TFPB$^-$ ions are likely to be accumulated only in the topmost layer until a limit potential when the topmost layer is fully occupied by TFPB$^-$ ions. Such a potential is significantly more positive than +0.20 V, judging from the EDL analysis described below. We note that the bilayer formation for TOMA$^+$ is different from "lattice saturation",[74] which is known to be one of the unique features of the EDL in IL, since absolute values of the potentials in the present study are not great enough to induce the saturation of ions in the topmost ionic layer.

The electron densities of the box (monolayer and bilayer) are 0.387 and 0.367 e Å^{-3} for $\Delta_{\mathrm{IL}}^{\mathrm{W}}\phi$ = +0.20 and = −0.27 V, respectively (Table 3). These electron densities are higher and lower than that for IL bulk (0.373 e Å^{-3}), respectively, supporting qualitative discussion described above. From these quantitative data, we can estimate the surface charge density of the IL side at the IL|W interface because electron density change from the bulk value can be caused by the accumulation and depletion of IL cations and anions in the EDL layer from the electrochemical point of view. Considering that the accumulation or depletion of ions leads to the charging

of IL|W interface, the surface charge density on the IL side of the interface, q_{IL}, may be estimated as follows,

$$q_{\mathrm{IL}} = q_{1,\max}\frac{d_{\mathrm{int}}}{d_1}\frac{\rho_{\mathrm{int}} - \rho_{\mathrm{IL}}}{\rho_{\mathrm{C}} - \rho_{\mathrm{IL}}} \tag{20}$$

where $q_{1,\max} = e/d_1^2$ is the absolute value of the surface charge density when the cation or anion are fully covered in the topmost layer. When $d_{\mathrm{int}} = d_1$, three cases that $\rho_{\mathrm{int}} = \rho_{\mathrm{A}}, \rho_{\mathrm{IL}}, \rho_{\mathrm{C}}$ corresponds to $q_{\mathrm{IL}} = -q_{1,\max}, 0, +q_{1,\max}$, respectively (note that $\rho_{\mathrm{IL}} = (\rho_{\mathrm{C}} + \rho_{\mathrm{A}})/2$). From the ρ_{int} and d_{int} values in Table 3, the q_{IL} values at +0.20 V and −0.27 V are estimated to be −1.2 and +1.2 μC cm^{-2}, respectively.

3.3 EDL model

To quantitatively discuss the obtained surface charge density, we performed model calculation using a mean-field theory for the EDL at the IL|W interface. The results of the calculation for the potential profile and the ionic concentration profiles around the IL|W interface at +0.20 V and −0.27 V are shown in Figs. 3 and 4, respectively. The EDL thickness in IL was found to be within topmost ionic layer (12.0 Å). This prediction from the present mean-field theory agrees with the XR results at +0.20 V where we found the high electron density box with the thickness of ionic monolayer. On the other hand, at −0.27 V, XR results illustrate bilayer feature of the EDL in IL, contradicting with the mean-field theory. Again, this can be explained by local and non-coulombic interaction between neighboring $TOMA^+$ ions. The mean-field theory does not incorporate such interaction, only considering global (averaged) and coulombic interaction. For the EDL in W in Figs. 3 and 4, the ionic concentrations are low enough, not to change the electron density on the W side of the interface to focus on the EDL in IL in the XR measurements.

Using the present EDL model the q_{IL} values were calculated to be −0.38 and +1.2 μC cm^{-2} at +0.20 and −0.27 V, respectively. The absolute value at +0.20 V is significantly smaller than that evaluated from XR (Table 3), while that at −0.27 V is the same. Note that this coincidence at −0.27 V is somewhat meaningless because we saw the mean-field theory breaking down at that potential due to the bilayer formation as described above. One possible reason for the deviation at +0.20 V is too thick inner layer in IL. $TOMA^+$ ions have asymmetric shape and the charged part of the ions can approach the IL|W interface closer than the ionic center. Therefore, we also performed model calculation of the EDL when the inner layer thickness on the IL side is zero as an extreme case (Figs. S1 and S2) and calculated the q_{IL} values (Table 3). The $|q_{\mathrm{IL}}|$ values become greater as expected since the inner layer capacitance for the IL side is neglected and the total capacitance of the IL|W interface becomes greater. However, the calculated $|q_{\mathrm{IL}}|$ value at +0.20 V, +0.56 μC cm^{-2}, is still significantly smaller than the experimentally evaluated value of $|q_{\mathrm{IL}}|$, +1.2 μC cm^{-2}. Another possibility for the deviation is the densification of the ionic layer as was observed at the IL|metal electrode interface.[75,98,99] The densification of the ionic layer would make us to overestimate the q_{IL} from eq 20 because the equation assumes that deviation of electron density from the bulk value only comes from the charge up of the interface. One may

modify eq 20, taking into account the densification factor, f,

$$q_{\mathrm{IL}} = q_{1,\max}\frac{d_{\mathrm{int}}}{d_1}\frac{\rho_{\mathrm{int}} - f\rho_{\mathrm{IL}}}{\rho_{\mathrm{C}} - \rho_{\mathrm{IL}}} \tag{21}$$

The f values were 1.024 and 1.019 to fit the experimental q_{IL} value at +0.20 V to 0.38 and 0.56 μC cm^{-2}, respectively, suggesting that the density of the topmost ionic layer is around 2% higher than in bulk at the potential.

In conclusion, x-ray reflectivity at the IL|W interface have been measured to probe the structure of the EDL in IL. In particular, IL-cation-accumulated bilayers has been confirmed when IL side of the interface is positively charged. The bilayer formation cannot be predicted from the mean-field theory, demonstrating the importance of local non-coulombic interaction between ions in the EDL in ILs. Data at various phase-boundary potentials will reveal more detailed EDL structure in ILs and such a study is in progress in our laboratory.

Acknowledgments

The authors appreciate discussion with and comments by Takashi Kakiuchi and are also grateful to Yuki Kitazumi and Eiji Minami for the synthesis of $Na^+[TFPB^-]$ and the measurements of the physicochemical properties of $[TOMA^+][TFPB^-]$, respectively. This work has been performed with the approval of SPring-8 (Proposal Nos. 2011A1187, 2011B1394, 2012A1257, 2012B1170, 2014B1058). This work was partly supported by Grant-in-Aids from the Ministry of Education, Culture, Sports, Science, and Technology, Japan (Nos. 21750075, 26248004, 26410149) and from the Hattori-Hokokai Foundation.

Appendix A. Supplementary data

The analysis of the fitting results using AIC and the calculation results of electrical double layer at the IL|W interface. Supplementary data to this article can be found online at http://******

Table 1: Parameters in the EDL calculation.

Symbol	Definition	Value	Unit
ϵ_{IL}	Relative permittivity in IL	10	–
ϵ_{W}	Relative permittivity in W	80	–
$c_{0,\mathrm{IL}}$	Ionic concentration in IL bulk	974 [a]	mol m^{-3}
$c_{0,\mathrm{W}}$	Ionic concentration in W bulk	0.1 or 0.01	mol m^{-3}
$d_{2,\mathrm{IL}}$	Inner layer thickness in IL	6 or 0	Å
$d_{2,\mathrm{W}}$	Inner layer thickness in W	3	Å
ν	Absolute value of charge number for ions	1	–
T	Absolute temperature	330	K
R	Gas constant	8.314	J K^{-1} mol^{-1}
F	Faraday constant	96485	C mol^{-1}
ϵ_0	Vacuum permittivity	8.8542	F m^{-1}

[a]Calculated using the molecular weight and the density of [TOMA$^+$][TFPB$^-$].

Table 2: Parameters obtained by fitting the curve from the MDC model to XR data at the [$TOMA^+$][$TFPB^-$]|air interface.

d (Å)	σ_0 (Å)	$\bar{\sigma}$ (Å)	σ_{surf} (Å)	f_{surf} (-)
12.0 ± 1.5	5.0 ± 0.2	3 ± 3	4.2 ± 1.0	0.77 ± 0.03

Table 3: Parameters obtained by fitting the curve from the one-box model to XR data at the [$TOMA^+$][$TFPB^-$]|W interface.

Component in W	$\Delta_{IL}^{W}\phi$	d_1	ρ_{int}	q_{IL} [c]	q_{IL} [d]	q_{IL} [e]
(-)	(V)	(Å)	(e Å^{-3})	(μC cm^{-2})	(μC cm^{-2})	(μC cm^{-2})
0.010 mM Na^+[$TFPB^-$]	+0.20[a]	11.7 ± 1.8	0.387 ± 0.003	−1.2	−0.38	−0.56
0.10 mM [$TOMA^+$]Cl^-	−0.27[b]	25.5 ± 1.0	0.367 ± 0.001	+1.2	+1.2	+2.8

[a] Estimated from $\Delta_{NB}^{W}\phi_{TFPB}^{0'}$ = +0.50 V[100] and c_{TFPB}^{W} = 1.0×10^{-5} M. [b] Estimated from $\Delta_{NB}^{W}\phi_{TOMA}^{0'}$ = −0.51 V[15] and c_{TOMA}^{W} = 1.0×10^{-4} M. [c] Calculated using eq 20. [d] Estimated using the EDL model with an inner layer thickness in IL of $d_1/2$. [e] Estimated using the EDL model with an inner layer thickness in IL of 0.

References

1 S. Dai, Y. H. Ju, and C. E. Barnes, *J. Chem. Soc., Dalton Trans.*, 1999 1201–1202.

2 A. E. Visser, R. P. Swatloski, W. M. Reichert, S. T. Griffin, and R. D. Rogers, *Ind. Eng. Chem. Res.*, 2000, **39**, 3596–3604.

3 M. L. Dietz, J. A. Dzielawa, I. Laszak, B. A. Young, and M. P. Jensen, *Green Chem.*, 2003, **5**, 682–685.

4 G.-T. Wei, Z. Yang, and C.-J. Chen, *Anal. Chim. Acta*, 2003, **488**, 183–192.

5 H. M. Luo, S. Dai, and P. V. Bonnesen, *Anal. Chem.*, 2004, **76**, 2773–2779.

6 K. Shimojo and M. Goto, *Anal. Chem.*, 2004, **76**, 5039–5044.

7 N. Nishi, H. Murakami, S. Imakura, and T. Kakiuchi, *Anal. Chem.*, 2006, **78**, 5805–5812.

8 J. H. Wang, D. H. Cheng, X. W. Chen, Z. Du, and Z. L. Fang, *Anal. Chem.*, 2007, **79**, 620–625.

9 S. R. Yousefi and F. Shemirani, *Anal. Chim. Acta*, 2010, **669**, 25–31.

10 J. M. Pringle, O. Ngamna, C. Lynam, G. G. Wallace, M. Forsyth, and D. R. Macfarlane, *Macromolecules*, 2007, **40**, 2702–2711.

11 K. Yao, W. Lu, X. Li, J. Wang, and J. Yuan, *Chem. Commun.*, 2013, **49**, 1398–1400.

12 N. Nishi, T. Kakinami, and T. Sakka, *Chem. Commun.*, 2015, **51**, 13638–13641.

13 C. Coll, R. H. Labrador, R. M. Mañez, J. Soto, F. Sancenón, M.-J. Seguí, and E. Sanchez, *Chem. Commun.*, 2005 3033–3035.

14 P. G. Boswell, E. C. Lugert, J. Rábai, E. A. Amin, and P. Bühlmann, *J. Am. Chem. Soc.*, 2005, **127**, 16976–16984.

15 N. Nishi, H. Murakami, Y. Yasui, and T. Kakiuchi, *Anal. Sci.*, 2008, **24**, 1315–1320.

16 H. Khani, M. K. Rofouei, P. Arab, V. K. Gupta, and Z. Vafaei, *J. Hazard. Mater.*, 2010, **183**, 402–409.

17 T. Ohtani, N. Nishi, and T. Kakiuchi, *J. Electroanal. Chem.*, 2011, **656**, 102–105.

18 C. Wardak and J. Lenik, *Sens. Actuator B-Chem.*, 2013, **189**, 52–59.

19 T. Kakiuchi and T. Yoshimatsu, *Bull. Chem. Soc. Jpn.*, 2006, **79**, 1017–1024.

20 T. Kakiuchi, *Electrochem. Commun.*, 2014, **45**, 37–39.

21 R. M. Lynden-Bell, J. Kohanoff, and M. G. Del Pópolo, *Faraday Discuss.*, 2005, **129**, 57–67.

22 A. Chaumont and G. Wipff, *Inorg. Chem.*, 2004, **43**, 5891–5901.

23 P. Vayssiere, A. Chaumont, and G. Wipff, *Phys. Chem. Chem. Phys.*, 2005, **7**, 124–135.

24 A. Chaumont, R. Schurhammer, and G. Wipff, *J. Phys. Chem. B*, 2005, **109**, 18964–18973.

25 G. Chevrot, R. Schurhammer, and G. Wipff, *Phys. Chem. Chem. Phys.*, 2006, **8**, 4166–4174.

26 N. Sieffert and G. Wipff, *J. Phys. Chem. B*, 2006, **110**, 13076–13085.

27 N. Sieffert and G. Wipff, *J. Phys. Chem. B*, 2006, **110**, 19497–19506.

28 A. Chaumont and G. Wipff, *J. Mol. Liq.*, 2007, **131**, 36–47.

29 A. Chaumont and G. Wipff, *J. Phys. Chem. C*, 2009, **113**, 18233–18243.

30 A. Chaumont and C. Wipff, *J. Phys. Chem. B*, 2010, **114**, 13773–13785.

31 C. Gaillard, V. Mazan, S. Georg, O. Klimchuk, M. Sypula, I. Billard, R. Schurhammer, and G. Wipff, *Phys. Chem. Chem. Phys.*, 2012, **14**, 5187–5199.

32 M. Klaehn, C. Stueber, A. Seduraman, and P. Wu, *J. Phys. Chem. B*, 2010, **114**, 2856–2868.

33 M. Sha, D. Niu, Q. Dou, G. Wu, H. Fang, and J. Hu, *Soft Matter*, 2011, **7**, 4228–4233.

34 M. H. Ghatee and A. R. Zolghadr, *J. Phys. Chem. C*, 2013, **117**, 2066–2077.

35 D. S. Frost and L. L. Dai, *Langmuir*, 2011, **27**, 11339–11346.

36 D. S. Frost, E. M. Nofen, and L. L. Dai, *Adv. Colloid Interface Sci.*, 2014, **206**, 92–105.

37 J. K. Konieczny and B. Szefczyk, *J. Phys. Chem. B*, 2015, **119**, 3795–3807.

38 N. Nishi, R. Ishimatsu, M. Yamamoto, and T. Kakiuchi, *J. Phys. Chem. C*, 2007, **111**, 12461–12466.

39 N. Nishi, M. Yamamoto, and T. Kakiuchi, *Bunsekikagaku*, 2007, **56**, 491–497.

40 T. Iwahashi, Y. Sakai, D. Kim, T. Ishiyama, A. Morita, and Y. Ouchi, *Faraday Discuss.*, 2012, **154**, 289–301.

41 T. Kakiuchi, N. Tsujioka, K. Sueishi, N. Nishi, and M. Yamamoto, *Electrochemistry*, 2004, **72**, 833–835.

42 N. Nishi, S. Imakura, and T. Kakiuchi, *J. Electroanal. Chem.*, 2008, **621**, 297–303.

43 Z. Samec, J. Langmaier, and T. Kakiuchi, *Pure Appl. Chem.*, 2009, **81**, 1473–1488.

44 T. Kakiuchi, F. Shigematsu, T. Kasahara, N. Nishi, and M. Yamamoto, *Phys. Chem. Chem. Phys.*, 2004, **6**, 4445–4449.

45 B. D. Fitchett, J. B. Rollins, and J. C. Conboy, *Langmuir*, 2005, **21**, 12179–12186.

46 R. Ishimatsu, F. Shigematsu, T. Hakuto, N. Nishi, and T. Kakiuchi, *Langmuir*, 2007, **23**, 925–929.

47 R. Ishimatsu, N. Nishi, and T. Kakiuchi, *Langmuir*, 2007, **23**, 7608–7611.

48 R. Ishimatsu, Y. Kitazumi, N. Nishi, and T. Kakiuchi, *J. Phys. Chem. B*, 2009, **113**, 9321–9325.

49 Y. Yasui, Y. Kitazumi, N. Nishi, and T. Kakiuchi, *J. Chem. Eng. Data*, 2010, **55**, 4463–4466.

50 L. G. Gouy, *J. Phys.*, 1910, **9**, 457–468.

51 D. L. Chapman, *Phil. Mag.*, 1913, **25**, 475–481.

52 O. Stern, *Z. Elektrochem.*, 1924, **30**, 508–516.

53 R. G. Horn, D. F. Evans, and B. W. Ninham, *J. Phys. Chem.*, 1988, **92**, 3531–3537.

54 M. Mezger, H. Schröder, H. Reichert, S. Schramm, J. S. Okasinski, S. Schöder, V. Honkimäki, M. Deutsch, B. M. Ocko, J. Ralston, M. Rohwerder, M. Stratmann, and H. Dosch, *Science*, 2008, **322**, 424–428.

55 R. Hayes, G. G. Warr, and R. Atkin, *Phys. Chem. Chem. Phys.*, 2010, **12**, 1709–1723.

56 S. Perkin, T. Albrecht, and J. Klein, *Phys. Chem. Chem. Phys.*, 2010, **12**, 1243–1247.

57 N. Nishi, Y. Yasui, T. Uruga, H. Tanida, T. Yamada, S. Nakayama, H. Matsuoka, and T. Kakiuchi, *J. Chem. Phys.*, 2010, **132**, 164705.

58 Y. Yokota, T. Harada, and K. Fukui, *Chem. Commun.*, 2010, **46**, 8627–8629.

59 N. Nishi, T. Uruga, H. Tanida, and T. Kakiuchi, *Langmuir*, 2011, **27**, 7531–7536.

60 Y. Lauw, M. D. Horne, T. Rodopoulos, V. Lockett, B. Akgun, W. A. Hamilton, and A. R. J. Nelson, *Langmuir*, 2012, **28**, 7374–7381.

61 R. Yamamoto, H. Morisaki, O. Sakata, H. Shimotani, H. Yuan, Y. Iwasa, T. Kimura, and Y. Wakabayashi, *Appl. Phys. Lett.*, 2012, **101**, 053122.

62 R. Köhler, J. Restolho, R. Krastev, K. Shimizu, J. N. Canongia Lopes, and B. Saramago, *J. Phys. Chem. Lett.*, 2011, **2**, 1551–1555.

63 X. Zhang, L. Lu, and Y. Cai, *Langmuir*, 2012, **28**, 9593–9600.

64 M. Rosa Castillo, J. M. Fraile, and J. A. Mayoral, *Langmuir*, 2012, **28**, 11364–11375.

65 Y. Yasui, Y. Kitazumi, R. Ishimatsu, N. Nishi, and T. Kakiuchi, *J. Phys. Chem. B*, 2009, **113**, 3273–3276.

66 T. Kakiuchi, Y. Yasui, Y. Kitazumi, and N. Nishi, *ChemPhysChem*, 2010, **11**, 2912–2918.

67 Y. Yasui, Y. Kitazumi, H. Mizunuma, N. Nishi, and T. Kakiuchi, *Electrochem. Commun.*, 2010, **12**, 1479–1482.

68 Y. Yasui, Y. Kitazumi, N. Nishi, and T. Kakiuchi, *J. Phys. Chem. B*, 2010, **114**, 11141–11148.

69 I. Bou-Malham and L. Bureau, *Soft Matter*, 2010, **6**, 4062–4065.

70 S. Makino, Y. Kitazumi, N. Nishi, and T. Kakiuchi, *Electrochem. Commun.*, 2011, **13**, 1365–1368.

71 M. Drüschler, N. Borisenko, J. Wallauer, C. Winter, B. Huber, F. Endres, and B. Roling, *Phys. Chem. Chem. Phys.*, 2012, **14**, 5090–5099.

72 N. Nishi, Y. Hirano, T. Motokawa, and T. Kakiuchi, *Phys. Chem. Chem. Phys.*, 2013, **15**, 11615–11619.

73 K. Motobayashi, K. Minami, N. Nishi, T. Sakka, and M. Osawa, *J. Phys. Chem. Lett.*, 2013, **4**, 3110–3114.

74 A. A. Kornyshev, *J. Phys. Chem. B*, 2007, **111**, 5545–5557.

75 N. Nishi, A. Hashimoto, E. Minami, and T. Sakka, *Phys. Chem. Chem. Phys.*, 2015, **17**, 5219–5226.

76 G. Luo, S. Malkova, S. Pingali, D. Schultz, B. Lin, M. Meron, T. Graber, R. Gebhardt, P. Vanysek, and M. Schlossman, *Faraday Discuss.*, 2005, **129**, 23–34.

77 G. Luo, S. Malkova, J. Yoon, D. G. Schultz, B. Lin, M. Meron, I. Benjamin, P. Vanysek, and M. L. Schlossman, *J. Electroanal. Chem.*, 2006, **593**, 142–158.

78 G. Luo, S. Malkova, J. Yoon, D. Schultz, B. Lin, M. Meron, I. Benjamin, P. Vanysek, and M. Schlossman, *Science*, 2006, **311**, 216–218.

79 N. Laanait, J. Yoon, B. Hou, P. Vanysek, M. Meron, B. Lin, G. Luo, I. Benjamin, and M. L. Schlossman, *J. Chem. Phys.*, 2010, **132**, 171101.

80 N. Laanait, M. Mihaylov, B. Hou, H. Yu, P. Vanysek, M. Meron, B. Lin, I. Benjamin, and M. L. Schlossman, *Proc. Natl. Acad. Sci. U. S. A.*, 2012, **109**, 20326–20331.

81 B. Hou, N. Laanait, H. Yu, W. Bu, J. Yoon, B. Lin, M. Meron, G. Luo, P. Vanysek, and M. L. Schlossman, *J. Phys. Chem. B*, 2013, **117**, 5365–5378.

82 N. Nishi, S. Imakura, and T. Kakiuchi, *Anal. Chem.*, 2006, **78**, 2726–2731.

83 H. Nishida, N. Takada, M. Yoshimura, T. Sonoda, and H. Kobayashi, *Bull. Chem. Soc. Jpn.*, 1984, **57**, 2600–2604.

84 Y. F. Yano, T. Uruga, H. Tanida, H. Toyokawa, Y. Terada, and H. Yamada, *J. Synchrot. Radiat.*, 2010, **17**, 511–516.

85 A. Braslau, P. S. Pershan, G. Swislow, B. M. Ocko, and J. Als-Nielsen, *Phys. Rev. A*, 1988, **38**, 2457–2470.

86 C. Gavach, P. Seta, and B. d'Epenoux, *J. Electroanal. Chem.*, 1977, **83**, 225–235.

87 E. J. W. Verwey and K. F. Niessen, *Phil. Mag.*, 1939, **25**, 435–446.

88 T. Kakiuchi and M. Senda, *Bull. Chem. Soc. Jpn.*, 1983, **56**, 1753–1760.

89 K. B. Oldham, *J. Electroanal. Chem.*, 2008, **613**, 131–138.

90 H. Akaike, *IEEE Trans. Autom. Control*, 1974, **AC19**, 716–723.

91 O. M. Magnussen, B. M. Ocko, M. J. Regan, K. Penanen, P. S. Pershan, and M. Deutsch, *Phys. Rev. Lett.*, 1995, **74**, 4444–4447.

92 H. D. Mo, G. Evmenenko, S. Kewalramani, K. Kim, S. N. Ehrlich, and P. Dutta, *Phys. Rev. Lett.*, 2006, **96**, 096107.

93 P. S. Pershan, S. E. Stoltz, O. G. Shpyrko, M. Deutsch, V. S. K. Balagurusamy, M. Meron, B. H. Lin, and R. Streitel, *Phys. Rev. B*, 2009, **79**, 115417.

94 T. Kakiuchi, N. Tsujioka, S. Kurita, and Y. Iwami, *Electrochem. Commun.*, 2003, **5**, 159–164.

95 T. Kakiuchi and N. Tsujioka, *Electrochem. Commun.*, 2003, **5**, 253–256.

96 N. Nishi, T. Kawakami, F. Shigematsu, M. Yamamoto, and T. Kakiuchi, *Green Chem.*, 2006, **8**, 349–355.

97 T. Pott and P. Meleard, *Phys. Chem. Chem. Phys.*, 2009, **11**, 5469–5475.

98 G.-B. Pan and W. Freyland, *Chem. Phys. Lett.*, 2006, **427**, 96–100.

99 N. Nishi, J. Uchiyashiki, R. Oogami, and T. Sakka, *Thin Solid Films*, 2014, **571**, 735–738.

100 Y. Yoshida, private communication.

Figure captions

Fig. 1 (a) Plot of $\log|\phi|^2$ as a function of q^2 at the [$TOMA^+$][$TFPB^-$]|air interface with error bars of one standard deviation (solid circle). The solid line is from the model fitting for the MDC model to the experimental plot. (b) Intrinsic electron density profile at the [$TOMA^+$][$TFPB^-$]|air interface using parameters obtained from the fitting listed in Table 2 (solid line). Gaussian profiles (dotted lines) correspond to ionic multilayers. Dashed line is the hypothetical case when $f_{\rm surf}$=1.

Fig. 2 (a) Plot of $\log|\phi|^2$ as a function of q^2 at the [$TOMA^+$][$TFPB^-$]|W interface with error bars of one standard deviation at +0.20 (red circle) and −0.27 (blue square) V. The red solid and blue dashed lines are from the model fitting for the one-box model to the experimental plots. The red dotted and blue dashed-dotted lines are the fitting results of the hypothetical case for the bilayer formation at +0.20 V and the monolayer formation at −0.27 V, respectively. (b) Intrinsic electron density profiles at the [$TOMA^+$][$TFPB^-$]|W interface at +0.20 (red solid line) and −0.27 (blue dashed line) V using parameters obtained from the fitting listed in Table 3. Vertical dotted lines at $z = 12, 24$ Å, are drawn to clarify the monolayer and bilayer thickness from the IL|W interface at $z = 0$.

Fig. 3 (a) Potential and (b) concentration profiles as a function of z at the IL|W interface when W contains 0.010 mM Na^+[$TFPB^-$] ($\Delta_{\rm IL}^{\rm W}\phi = +0.20$ V) with $d_{2,\rm IL} = 6$ Å. The vertical dashed lines at $z = -3, 0, 6,$ and 12 Å mean the boundary between the diffuse layer and the inner layer in W, the IL|W interface, the boundary between the diffuse layer and the inner layer in IL, and the boundary between topmost ionic layer and the second ionic layer, respectively.

Fig. 4 (a) Potential and (b) concentration profiles as a function of z at the IL|W interface when W contains 0.10 mM [$TOMA^+$]Cl^- ($\Delta_{\rm IL}^{\rm W} = -0.27$ V) with $d_{2,\rm IL} = 6$ Å. The vertical dashed lines at $z = -3, 0, 6,$ and 12 Å mean the boundary between the diffuse layer and the inner layer in W, the IL|W interface, the boundary between the diffuse layer and the inner layer in IL, and the boundary between topmost ionic layer and the second ionic layer, respectively.

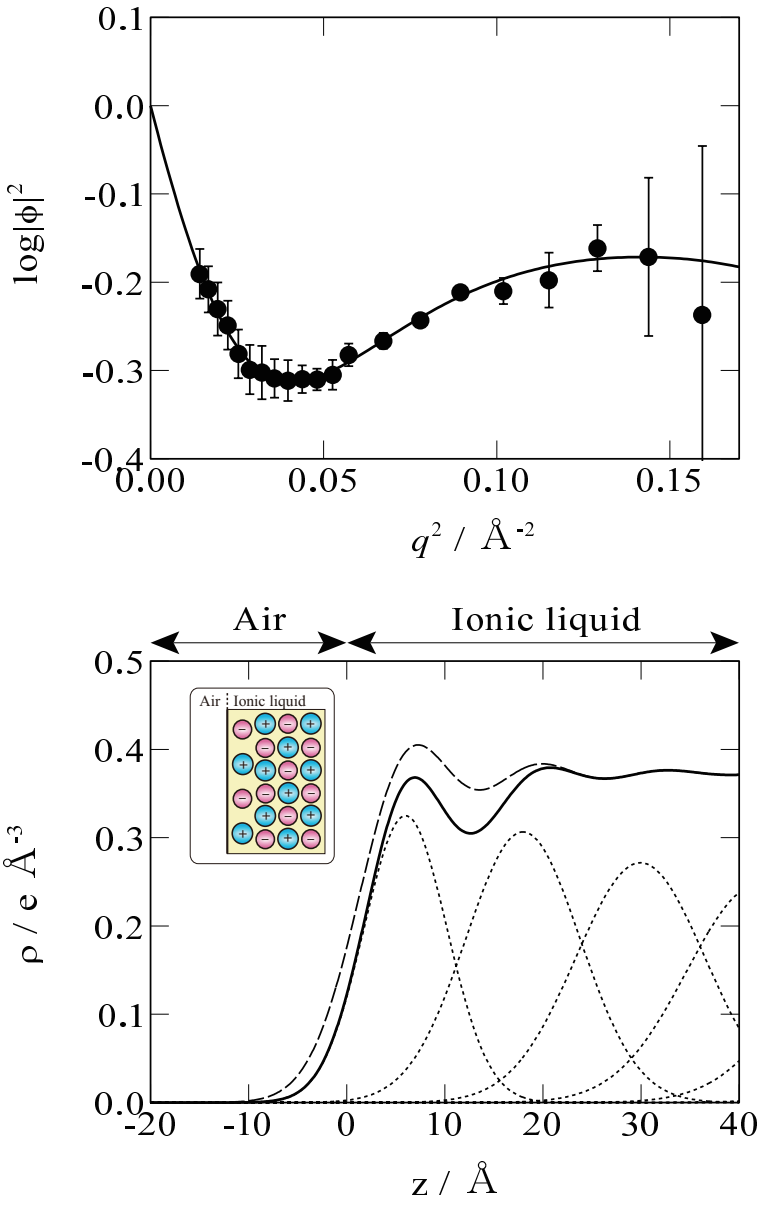

Fig. 1 (Nishi et al.)

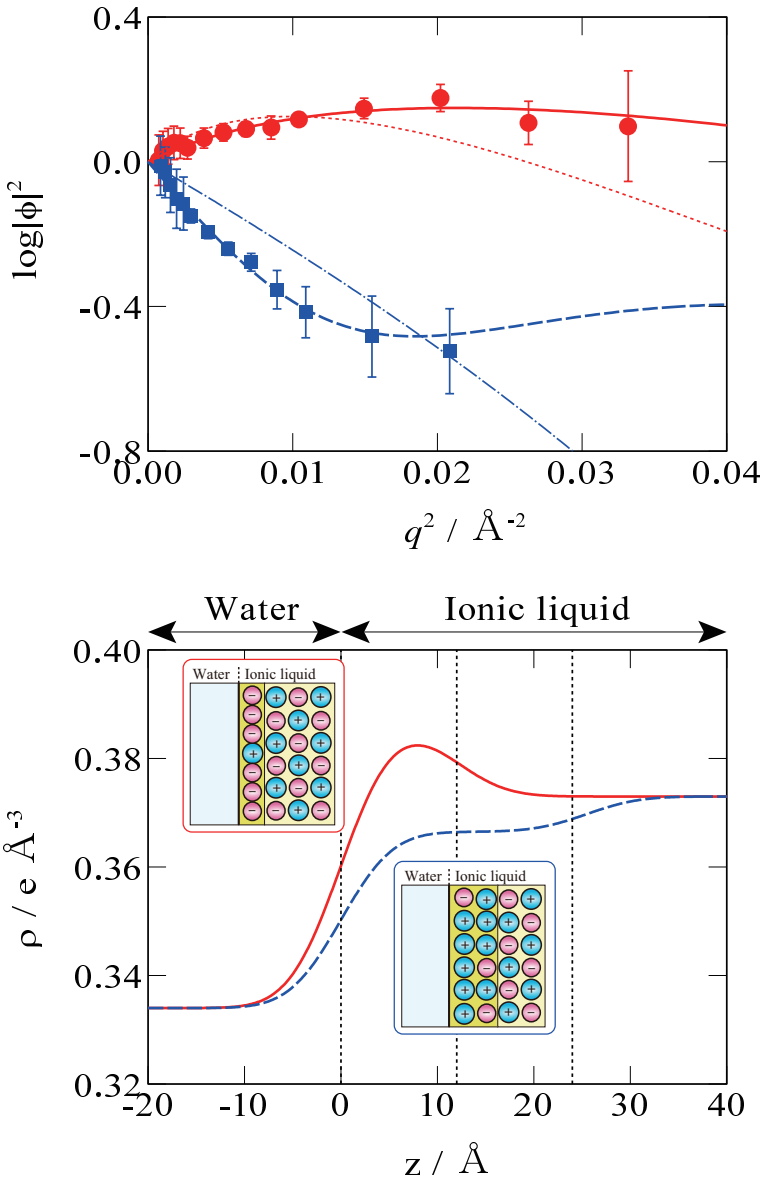

Fig. 2 (Nishi et al.)

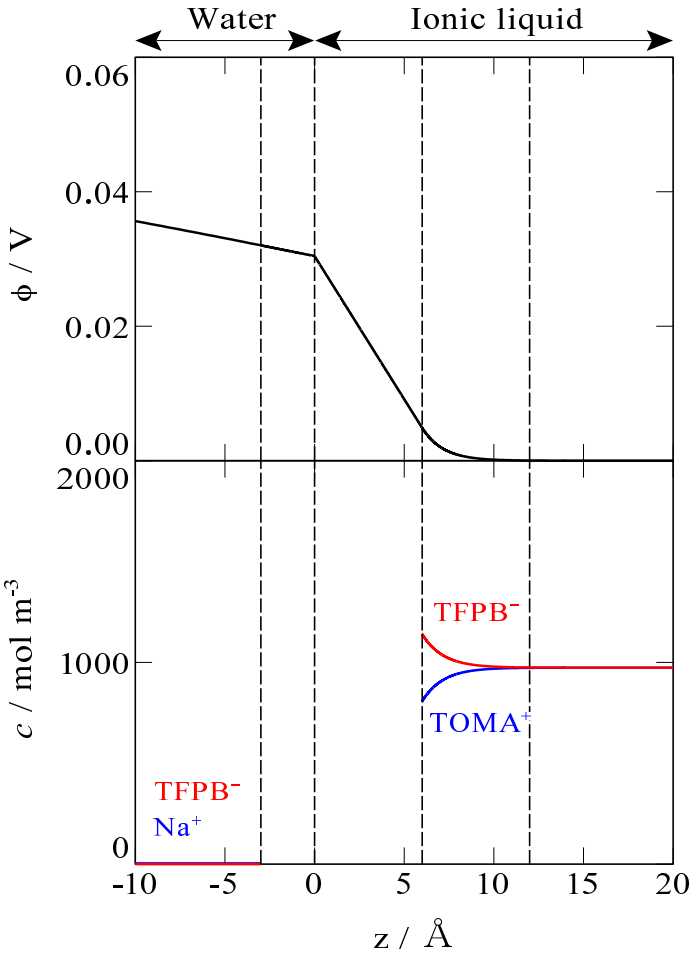

Fig. 3 (Nishi et al.)

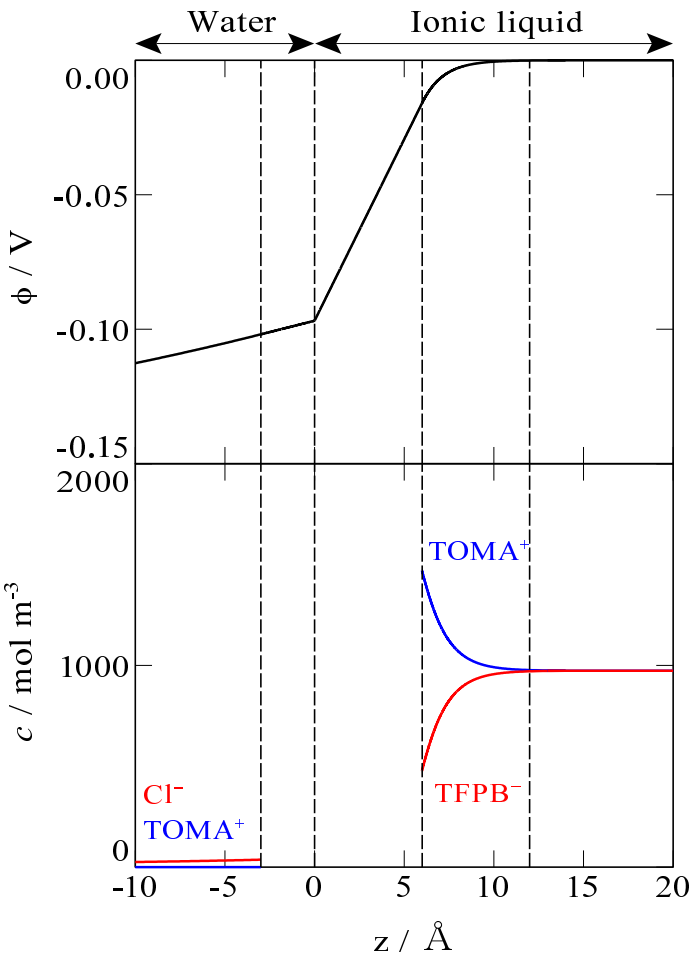

Fig. 4 (Nishi et al.)